NANO LETTERS

2008
Vol. 8, No. 3
775-779

InP Nanowire/Polymer Hybrid Photodiode

Clint J. Novotny, Edward T. Yu, and Paul K. L. Yu*

Department of Electrical and Computer Engineering, University of California-San Diego, La Jolla, California 92093

Received September 14, 2007; Revised Manuscript Received December 10, 2007

ABSTRACT

A novel design is presented for a nanowire/polymer hybrid photodiode. n-InP nanowires are grown directly onto an indium tin oxide (ITO) electrode to increase carrier collection efficiency and to eliminate the need for an expensive substrate. Experiments show that an ohmic contact is achieved between the nanowires and the ITO electrode. The nanowires are then enveloped by a high hole mobility conjugated polymer, poly(3-hexylthiophene). Compared to the control polymer-only device, the inclusion of InP nanowires increases the forward bias current conduction by 6−7 orders of magnitude. A high rectification ratio of 155 is achieved in these photodiodes along with a low ideality factor of 1.31. The hybrid device produces a photoresponse with a fill factor of 0.44, thus showing promise as an alternative to current polymer solar cell designs.

Semiconductor nanowires (NWs) have gained much attention over the course of the past decade. Their unique geometry leads to a large surface area to volume ratio, which has been exploited in devices such as biological and chemical sensors.[1–4] In the field of renewable energy, inorganic–organic hybrid photovoltaic devices based on conjugated polymers have generated a lot of attention because of their low cost and scalability to large-area devices. Nanorods,[5] nanoparticles,[6,7] and carbon nanotubes[8,9] have been dispersed in conjugated polymer hybrid solar cells as well as in nanowire-based dye-sensitized solar cells[10,11] to improve carrier mobility and collection efficiency. Compared to silicon or III−V substrates, the use of glass or plastic in these systems allows for a much more cost-efficient solution. However, one of the problems that many of these devices face is poor carrier transport.[12] In the case of nanorods or nanoparticles embedded in a polymer, carriers must hop from one site to the next as they are transported through the host material. This random pathway leads to an increase in the probability of recombination and thus a decrease in the overall photoconversion efficiency. To overcome this problem, groups have attempted to improve the alignment of the NWs by using intermediate steps such as template-assisted growth[13] and NW growth on an intermediate layer on top of the metal oxide.[14]

In this paper, we demonstrate an efficient carrier transport polymer hybrid system that does not require any intermediate step. This is achieved by growing NWs directly onto a metal oxide and enveloping the NWs with a conjugated polymer. Efficient carrier collection requires the photoinduced excitons to dissociate into free carriers that are then transported to their respective electrodes. With a bilayer polymer device structure (back-to-back polymer layers), only the excitons near that junction will split into electrons and holes. All other excitons produced in the polymer will be lost to recombination. Bulk organic heterojunction solar cells attempt to address this issue by blending two polymers to create junctions through the active layer. In our device, there are a very large number of junctions throughout the entire polymer matrix provided by the penetrating NWs, thus enhancing the probability of excitons dissociating at an interface. Furthermore, carriers created in the NWs have a direct pathway to the electrode and do not have to rely on carrier hopping. Therefore, this hybrid device has a more efficient and defined pathway for carrier collection. Because the mobility in the semiconductor material is several orders of magnitude higher than that of the polymer, carrier transport will be much more efficient. Direct growth of NWs onto the electrode will thus improve device performance, reduce the problem of reproducibility of contacts to NWs, and provide a method of NW growth that does not use expensive substrates such as Si or InP.

In this paper, we present the successful growth of n-InP NWs on ITO-coated glass substrates and show that we achieve an ohmic contact, thus providing an effective pathway for carriers. The effects of including the NWs into the polymer are explored and a comparison of the dark and light response of the device is made.

First, 250–300 nm of ITO was sputtered onto a glass substrate using a Denton Discovery 18 sputter system. Two depositions were done such that the top, bottom, and sides

* Corresponding author. E-mail: yu@ece.ucsd.edu.

10.1021/nl072372c CCC: $40.75
Published on Web 02/12/2008

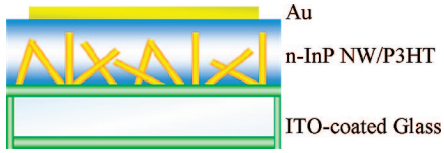

Figure 1. Nanowire−polymer hybrid device schematic.

of the glass substrate were covered, providing a continuous layer around the glass. Then n-InP NWs were grown on the ITO-coated glass substrates in a horizontal MOCVD reactor at a pressure of 100 torr. Trimethylindium (TMIn) and phosphine (PH_3) were used as the group III and V sources, respectively, with hydrogen as the carrier gas. The growth temperature was 425 °C with an input V/III ratio of 100. n-Type NWs were doped using a disilane source (25 ppm in hydrogen). The NWs nucleated and grew from indium droplets that formed on the surface. Details of this self-assembly growth process are given elsewhere.[15] NW growth characterization was carried out using a Phillips XL30 environmental scanning electron microscope (SEM), operating at 20 kV. The high hole mobility conjugated polymer used was poly(3-hexylthiophene) (P3HT), obtained from Plextronics, with >99% head-to-tail regioregularity. The P3HT was dissolved in 1,2,4-trichlorobenzene at concentrations ranging from 1 to 10 mg/mL. The use of this high boiling point solvent has been shown to yield an increase in the mobility and overall device performance.[16] All solutions were heated at 70 °C for 45 min before being filtered through a 0.45 μm pore size membrane syringe filter. P3HT was drop-cast onto the NW/ITO/glass samples and allowed to dry overnight in a desiccator under vacuum. The samples were then annealed at 120 °C for 1.5 h under vacuum ($<10^{-6}$ Torr) followed by a sputter deposition of 200 nm of gold. Current–voltage ($I-V$) measurements were carried out using an HP4156 parameter analyzer. An Oriel Instruments solar simulator, model 66902, was used to illuminate the devices using a AM 1.5 filter.

To the best of our knowledge, this is the first demonstration of InP NW growth directly onto an electrode. In contrast to conventional nanowire device fabrication approaches that typically suffer from a difficulty in the reproducibility of contacts to individual NWs,[17,18] this approach allows for a large number of NWs to grow directly onto the electrode, thus improving the reproducibility of our device and offering an alternative to electron beam lithography. Instead of relying on a single NW for the device, a very large number of NWs contribute to the carrier transport. Therefore, the overall performance of the device is based on the statistical average of the NWs rather than a single NW, leading to an enhanced reproducibility.

Figure 2 is an SEM image, taken at a tile of 45°, of as-grown n-InP NWs on ITO. The diameters of these NWs range from 40 to 80 nm and the lengths range from 1 to 3 μm. Unlike InP NW growth on InP(111)B, there is no single growth direction on ITO. This is due to the random orientation of the domains within the polycrystalline ITO layer. Studies have shown that similar "off-angle" InP NW growth can occur on various substrates other than InP by

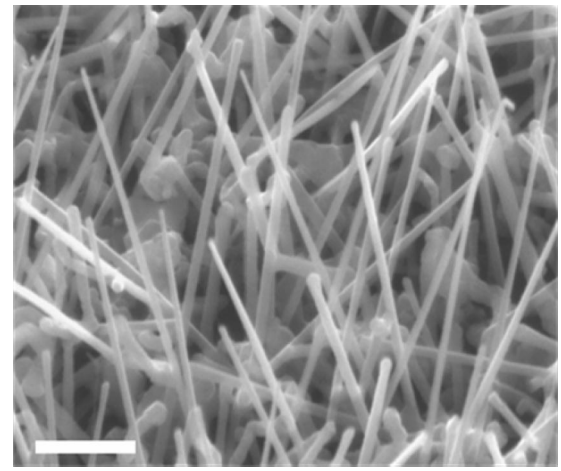

Figure 2. SEM image of n-InP NW growth on ITO taken at a 45° tilt with scale bar of 500 nm.

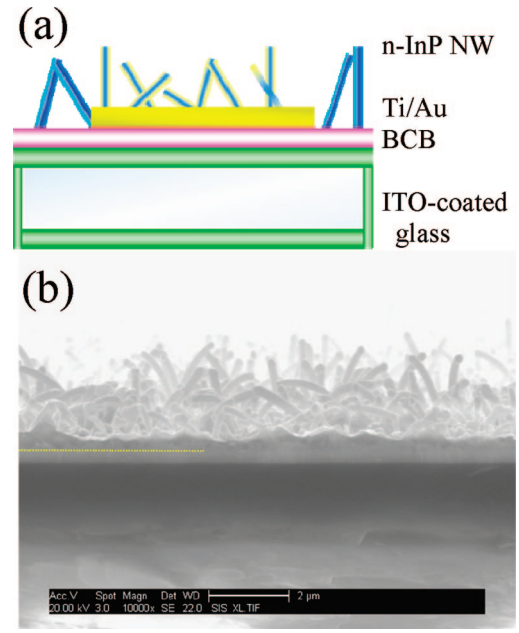

Figure 3. (a) Device schematic of NW/ITO interface test. (b) SEM image take at 90° tilt of the cross section of the NW/ITO test structure. The yellow dotted line delineates the ITO layer interface.

relying on short-range ordering of the polycrystalline substrate.[19] The NWs do grow away from the substrate, thus providing a structure that can penetrate several micrometers into the polymer matrix. To test the ITO/NW interface, $I-V$ measurements were conducted to determine the type of contact that is achieved. Figure 3a shows the device schematic for this test structure in which 200 nm of benzocyclobutene (BCB) is spun onto the NW/ITO sample. BCB has excellent reflow and planarization properties. After a 1 h anneal at 250 °C, BCB becomes very planar with very few pinholes. A short oxygen plasma etch is then performed to remove residual BCB from the sides of the NWs. A layer of titanium (10 nm) followed by gold (200 nm) is sputtered onto this sample and then undergoes rapid thermal annealing (RTA) for 1 min at 400 °C. This anneal allows for the contact to alloy with the NWs. A cross section of the final test

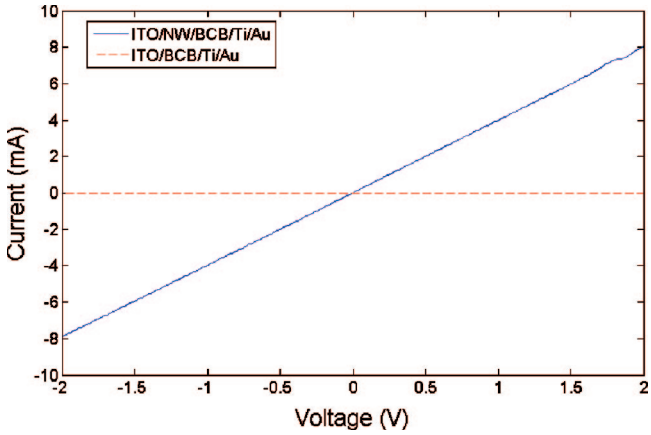

Figure 4. $I-V$ results of sample corresponding to Figure 3a without NWs (red dash) and with NWs (blue).

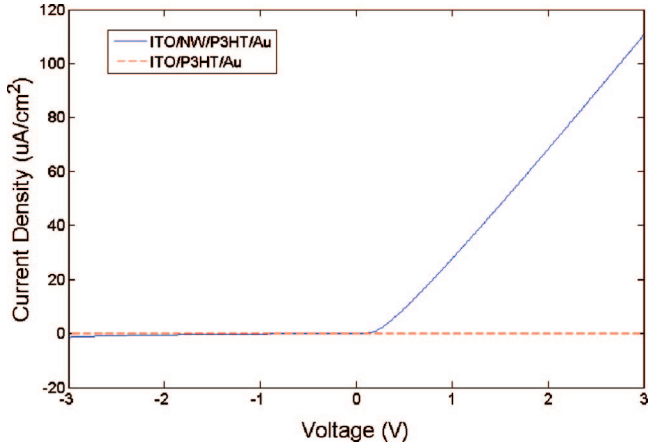

Figure 5. Dark measurement of samples corresponding to Figure 1 without NWs (red dash) and with (blue) NWs.

structure is shown in Figure 3b, showing that the BCB layer provides a continuous barrier between the Ti/Au and ITO electrodes.

The $I-V$ measurement is carried out by probing both the ITO/NW interface and the Au/Ti/NW interface. As seen in Figure 4, BCB is very insulating, and a measurement done on a control sample without NWs provides no current through the BCB layer (measured curve is similar to an open circuit measurement). However, the inclusion of NWs leads to shorting between the ITO and Ti/Au contacts. No rectification is seen in this measurement. Without any observed Schottky barrier, we thus conclude that the growth of NWs to the ITO electrode leads to an ohmic contact that will allow for efficient carrier collection at this electrode. While an individual NW will have a large resistance due to their small footprint, the resistance of a large number of NWs will add in parallel and thus produce a much smaller overall device resistance.

$I-V$ measurements were performed to analyze the effects of the inclusion of NWs to the conjugated polymer, P3HT. Control samples consist of a 4–6 μm thick layer of P3HT sandwiched between the ITO and Au contacts. The structure of the NW/P3HT samples is shown in Figure 1. Figure 5 depicts dark measurements performed on both a control

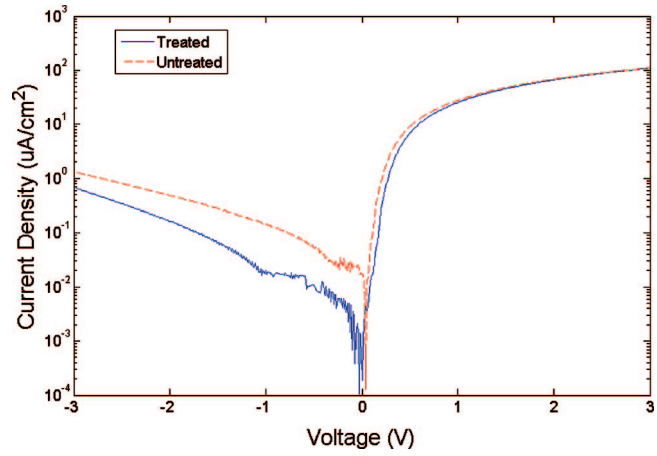

Figure 6. Semilog plot of dark measurement of untreated NW/P3HT sample (red dash) and "treated" (blue) sample that underwent an ammonium sulfide dip.

sample and a hybrid NW/P3HT sample. For the control sample, very little current (on the order of pA) passes through the polymer layer between the ITO and Au electrodes. However, the inclusion of NWs greatly enhances the current through the device. The NW/P3HT device has a current density of 110 μA/cm^2 at 3 V and a very low current in the negative voltage regime. This inclusion of the NWs increases the forward bias current by 6−7 orders of magnitude. The observed p−n junction behavior originates from the interface between the high hole mobility conjugated polymer and the n-doped NWs. The P3HT layer does not short the ITO and Au electrodes, as can be seen by the very low current of the P3HT only sample in Figure 5. However, care had to be taken to ensure the polymer completely embedded the NWs such that the NWs did not short the two electrodes. The height of the NWs was measured using SEM and the thickness of the P3HT was modified accordingly. Thus, only P3HT was in contact to the Au electrode.

The performance of two NW/polymer diodes is plotted in Figure 6 on a semilog scale. The first sample, labeled "untreated", has the same layer structure from Figure 5 of glass/ITO/NW/P3HT/Au. The second sample, labeled "treated", underwent an ammonium sulfide dip after the growth of the NWs. By passivating the InP surface with sulfur, unwanted nonradiative recombination at the surface of the NWs can be reduced.[20–22] Layers of P3HT and then Au were deposited on the sulfur-treated NW sample following the same procedure as the untreated sample. The current density–voltage ($J-V$) response of these diodes can be modeled using the ideal diode equation:[23]

$$J = J_{sat}(e^{V/nV_t} - 1) \quad (1)$$

where J_{sat} is the reverse saturation current density, n is the ideality factor, and V_t is the thermal voltage (26 mV). This equation is used to describe behavior due to a single p−n junction. In the case of the NW/polymer devices, there are many p−n junctions throughout the device and thus the overall $J-V$ measurement will be a sum of these characteristics. The ideality factor is a figure of merit that describes the recombination behavior of the device. A device governed purely by diffusion current will have $n = 1$ (ideal diode),

Table 1. $J-V$ Results for Untreated and Ammonium Sulfide Treated Samples[a]

	untreated	treated
n	1.31	1.37
J_{sat} (A/cm^2)	3.9×10^{-9}	8.5×10^{-10}
RR	81	155
V_{on} (V)	0.32	0.38
V_{oc} (V)	0.20	0.18
J_{sc} (A/cm^2)	3.3×10^{-6}	2.2×10^{-6}
FF	0.41	0.44

[a] Diode figures of merit: ideality factor (n), reverse saturation current density (J_{sat}), rectification ratio (RR), turn-on voltage (V_{on}). Solar cell figures of merit: open circuit voltage (V_{oc}), short circuit current density (J_{sc}), and fill factor (FF).

while a device dominated by recombination will have $n = 2$. Recombination can occur at interfaces where opposing charge carriers can meet. Thus, the ideality factor is a manifestation of the density and quality of interfaces in hybrid devices.[24,25] Bulk heterojunction solar cells that rely on interfaces due to blended polymers show that the use of different solvents alters the morphology of the interfaces and is usually reflected in the differing ideality factors.[26] The second component governing the behavior of the diode is the reverse saturation current density, which measures how many carriers can overcome the energetic barrier created by the p−n junction in the reverse bias direction. It represents the minority carrier density near the interface and depends on the minority carrier diffusion lengths, coefficients, and concentrations as well as the surface recombination velocities and junction design.[27] Optimized diodes will try to minimize the reverse saturation current to improve overall rectification of the device.

By taking the natural log of eq 1, we can approximate the linear region of the forward bias in Figure 6 as:

$$\ln J = \frac{1}{V_t}\frac{1}{n}V + \ln J_{sat} \tag{2}$$

Thus, the slope and intercept of the fitted line to this region provide the values of n and J_{sat}, respectively. The ideality factor for untreated and treated samples was 1.31 and 1.37, respectively. Thus, a large amount of the current is due to diffusion and is not dominated by recombination. The small variations seen in these values can be attributed to the variation in NW density and dimensions from the different growths. The reverse saturation current density showed a decrease by almost a factor of 5 from 3.9×10^{-9} to 8.5×10^{-10} A/cm^2 for the untreated and treated samples, respectively. Furthermore, the rectification ratio (current ratio measured at +3 V versus −3 V) increased by almost a factor of 2 from 81 to 155 for the untreated and treated samples, respectively. Therefore, by passivating the surface, leakage pathways can be reduced in this system and achieve a rectification of over 2 orders of magnitude. This high degree of rectification will improve carrier transport in the device by eliminating some of the leakage sources that are often seen in polymer hybrid solar cells. Finally, the turn-on voltages were estimated to be 0.32 and 0.38 V for the untreated and treated samples, respectively. These values were determined by extending the linear region of the $I-V$ curves to the horizontal axis. The low threshold values indicate that these devices will have fairly low power consumption. The summary of these values can be found in Table 1.

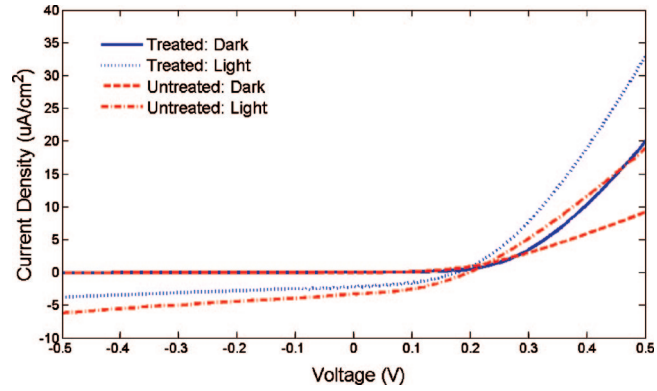

Figure 7. Comparison of light and dark measurement for untreated (dark: red dash; light: red dot−dash) and ammonium sulfide treated samples (dark: solid blue; light: blue dot).

Illumination of the diode alters eq 1 to:

$$J = J_{sat}(e^{V/nV_t} - 1) - J_L \tag{3}$$

where J_L represented the photogenerated current. Thus, the measured dark current will shift downward under illumination. Figure 7 compares the response of the devices to dark and light conditions, confirming the presence of a photogenerated current. This photoresponse is necessary for any possible photovoltaic application of this NW growth. For solar cell applications, the figures of merit are the short circuit current density (J_{sc}), open circuit voltage (V_{oc}), rectification ratio (RR), and fill factor (FF). The values for these devices are also summarized in Table 1. The fill factor is calculated by:[28]

$$FF = \frac{J_m V_m}{J_{sc} V_{oc}} \tag{4}$$

where $J_m V_m$ is the maximum power point. The short circuit density (current density at zero voltage) for the treated and untreated samples was 2.2 and 3.3 μA/cm^2, respectively. The open circuit voltages (voltage at zero current density) for treated and untreated were 0.18 and 0.20 V, respectively, with fill factors of 0.44 and 0.41, respectively.

For most polymer solar cells, the thickness of the polymer layer must be kept to a few hundred nanometers due to the poor mobility in these materials. As the layer thickness decreases, however, the absorption of the incoming light also decreases. In this work, the thickness of the P3HT varied between 4 and 6 μm depending on the sample. As seen in Figure 5, this thickness is too large for carriers to survive in P3HT only. However, the inclusion of the NWs allows for improved conduction and thus removes the requirement of a thin layer. Therefore, hybrid NW/polymer devices can have an improved absorption due to the mobility of carriers in the InP NWs.

The low values of the short circuit current will limit the overall efficiency of these devices. To overcome some of the loss mechanisms in this device, further experiments are required to optimize the performance. Because the P3HT is drop-cast, the thickness of this polymer varies across the sample. In some areas, there is a large gap between the tips of the nanowires and the gold electrode. An improved polymer deposition technique, such as dip-coating, may allow for a more

uniform layer. Dry etching of the polymer layer may also be a viable method to control the polymer layer thickness. Future experiments are planned to examine the dependency of the short circuit current on the thickness of the polymer between the NW tips and the Au contact. Because of the low mobility in the polymer, many of the carriers are lost to recombination. This leads to a reduction in the overall short circuit current. The interface between the NWs and the polymer is also a leakage source. As seen by the enhanced rectification after sulfur passivation, the bonding between the surface states of the NWs and the side chains of the polymer can have a large effect on the short circuit current, and thus the overall device performance and is crucial to the optimization of this device. Further experiments are planned to improve this interface, and thus the overall charge transfer between the two materials by studying the device performance as a function of the surface treatment of the NWs.

In conclusion, we have shown that our NW/polymer hybrid devices have very good diode characteristics. InP NW growth directly onto an ITO electrode provides an ohmic contact for efficient carrier collection. The inclusion of NWs to P3HT increases current through the device and provides efficient pathways for the carriers. High rectification ratios, low ideality factors, and improved reverse saturation currents were achieved as well as a photoresponse from the NW/P3HT hybrid photodiode. By optimizing the thickness of the polymer between the tips of the NWs to the Au electrode as well as the interface between the NW surface states and the polymer side chains, the overall efficiency of the device can be improved. We believe this system can be a promising alternative to current solar cell technology.

Acknowledgement. This work was supported by the National Science Foundation under Program nos. ECS0307247 and ECS0506092. We thank Peter Matheu, Daniel Derkacs, and Swee Hoe Lim for their assistance with the solar simulator setup.

References

(1) Cui, Y.; Wei, Q.; Park, H.; Lieber, C. M. *Science* **2001**, *293*, 1289.
(2) Zheng, G.; Patolsky, F.; Cui, Y.; Wang, W. U.; Lieber, C. M. *Nat. Biotechnol.* **2005**, *23*, 1294.
(3) Zhang, D.; Liu, Z.; Li, C.; Tang, T.; Liu, X.; Han, S.; Lei, B.; Zhou, C. *Nano Lett* **2004**, *4*, 1919.
(4) Hsueh, T. J.; Chang, S. J.; Hsu, C. L.; Lin, Y. R.; Chen, I. C. *Appl. Phys. Lett.* **2007**, *91*, 053111.
(5) Huynh, W. U.; Dittmer, J. J.; Alivisatos, A. P. *Science* **2002**, *295*, 2425.
(6) Arici, E.; Hoppe, H.; Schäffler, F.; Meissner, D.; Malik, M. A.; Sariciftci, N. S. *Thin Solid Films* **2004**, *612*, 451–452.
(7) Plass, R.; Pelet, S.; Krueger, J.; Gratzel, M. *J. Phys. Chem. B* **2002**, *106*, 7578.
(8) Kymakis, E.; Amaratunga, G. A. J. *Appl. Phys. Lett.* **2002**, *80*, 112.
(9) Miller, J.; Hatton, R. A.; Silva, S. R. P. *Appl. Phys. Lett.* **2006**, *89*, 133117.
(10) Law, M.; Greene, L. E.; Johnson, J. C.; Saykally, R.; Yang, P. *Nat. Mater.* **2005**, *4*, 455.
(11) Baxter, J. B.; Walker, A. M.; van Ommering, K.; Aydil, E. S. *Nanotechnology* **2006**, *17*, S304.
(12) Greenham, N. C.; Peng, X.; Alivisatos, A. P. *Phys. Rev. B* **1996**, *54*, 17628.
(13) Kang, Y.; Park, N. G.; Kim, D. *Appl. Phys. Lett.* **2005**, *86*, 113101.
(14) Ravirajan, P.; Peiro, A. M.; Nazeeruddin, M. K.; Graetzel, M.; Bradley, D. D. C.; Durrant, J. R.; Nelson, J. *J. Phys. Chem. B* **2006**, *110*, 7635.
(15) Novotny, C.; Yu, P. K. L. *Appl. Phys. Lett.* **2005**, *87*, 203111.
(16) Chang, J. F.; Sun, B.; Breiby, D. W.; Nielsen, M. M.; Sölling, T. I.; Giles, M.; McCulloch, I.; Sirringhaus, H. *Chem. Mater.* **2004**, *16*, 4772.
(17) Langford, R. F.; Wang, T. X.; Thornton, M.; Heidelberg, A.; Sheridan, J. G.; Blau, W.; Leahy, R. *J. Vac. Sci. Technol., B* **2006**, *24*, 2306.
(18) Stern, E.; Cheng, G.; Klemic, J. F.; Broomfield, E.; Turner-Evans, D.; Li, C.; Zhou, C.; Reed, M. A. *J. Vac. Sci. Technol., B* **2006**, *24*, 231.
(19) Kobayashi, N. P.; Wang, S. Y.; Santori, C.; Williams, R. S. *Appl. Phys. A: Mater. Sci. Process.* **2006**, *85*, 1.
(20) Bessolov, V. N.; Lebedev, M. V.; Zahn, D. R. T. *Semiconductors* **1999**, *33*, 416.
(21) Ishimura, H.; Sasaki, K.; Tokuda, H. *Inst. Phys. Conf. Ser.* **1990**, *106*, 405.
(22) Iyer, R.; Lile, D. L. *Appl. Phys. Lett.* **1991**, *59*, 437.
(23) Sze, S. M. *Physics of Semiconductor Devices*, 2nd ed.; Wiley: New York, 1981.
(24) Schilinsky, P.; Waldauf, C.; Brabec, C. J. *Adv. Funct. Mater.* **2006**, *16*, 1669.
(25) Waldauf, C.; Scharber, M. C.; Schilinsky, P.; Hauch, J. A.; Brabec, C. J. *J. Appl. Phys.* **2006**, *99*, 104503.
(26) Waldauf, C.; Schilinsky, P.; Hauch, J.; Brabec, C. J. *Thin Solid Films* **2004**, *503*, 451–452.
(27) Rogalski, A.; Adamiec, K.; Rutkowski, J. *Narrow-Gap Semiconductor Photodiodes*; SPIE Press: Bellingham, WA, 2000.
(28) Fonashi, S. J. *Solar Cell Device Physics*; Academic Press: London, 1981.

NL072372C